PPGSpotter: Personalized Free Weight Training Monitoring Using Wearable PPG Sensor

Xiaochen Liu*   Fan Li*   Yetong Cao*   Shengchun Zhai*   Song Yang*   Yu Wang†

* School of Computer Science and Technology, Beijing Institute of Technology, China

† Department of Computer and Information Sciences, Temple University, USA

Email: {xiaochenliu, fli, yetongcao, shengchunzhai, S.Yang}@bit.edu.cn, wangyu@temple.edu

Abstract—Free weight training (FWT) is of utmost importance for physical well-being. However, the success of FWT depends heavily on choosing the suitable workload, as improper selections can lead to suboptimal outcomes or injury. Current workload estimation approaches rely on manual recording and specialized equipment with limited feedback. Therefore, we introduce *PPGSpotter*, a novel PPG-based system for FWT monitoring in a convenient, low-cost, and fine-grained manner. By characterizing the arterial geometry compressions caused by the deformation of distinct muscle groups during various exercises and workloads in PPG signals, *PPGSpotter* can infer essential FWT factors such as workload, repetitions, and exercise type. To remove pulse-related interference that heavily contaminates PPG signals, we develop an arterial interference elimination approach based on adaptive filtering, effectively extracting the pure motion-derived signal (MDS). Furthermore, we explore 2D representations within the phase space of MDS to extract spatiotemporal information, enabling *PPGSpotter* to address the challenge of resisting sensor shifts. Finally, we leverage a multi-task CNN-based model with workload adjustment guidance to achieve personalized FWT monitoring. Extensive experiments with 15 participants confirm that *PPGSpotter* can achieve workload estimation (0.59 kg RMSE), repetitions estimation (0.96 reps RMSE), and exercise type recognition (91.57% F1-score) while providing valid workload adjustment recommendations.

I. INTRODUCTION

Free weight training (FWT) has attained remarkable popularity owing to its salient role in fostering muscular strength, physical well-being, and emotional health. For example, in the United States, 78.4 million adults participate in FWT two or more sessions per week [1], illustrating the extensive participation worldwide. Moreover, with the increasing health awareness among individuals, FWT engagement is projected to increase substantially in the forthcoming years. During the FWT process, selecting an appropriate workload is crucial for achieving training goals. Experts and institutions emphasize the need for individuals to determine suitable training workloads based on their specific circumstances [2]: excessive workload may lead to injury, while inadequate workload may hamper progress. Based on this, numerous training workload models have been proposed, necessitating specialized knowl-
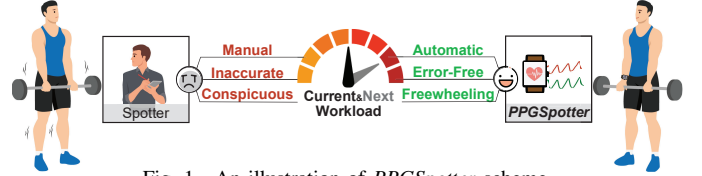
Fig. 1. An illustration of *PPGSpotter* scheme.

edge to determine optimal workload and workload adjustment. However, expertise engagement presents notable challenges to effective FWT execution, contributing to a significant barrier for many individuals. For instance, research [3] finds that more than 80% of participants failed to select the appropriate training workload without the supervision of a personal coach.

Nowadays, there have been significant developments in fitness assistance solutions [4]–[7], which offer precise and personalized feedback for sports like jogging, body-weight training, and high-intensity interval training. However, research in the field of FWT assisting lags behind. Most individuals still rely on manual methods to record, calculate, and adjust their workloads using various workload adjustment models [8]. To address this, researchers have attempted various devices for automatic workload estimation, including dedicated equipment-based solutions (e.g., smart adjustable dumbbells [9], RFID tags [10], and magnetic-cum-accelerometer [11]) and wearable-device-based solutions (e.g., surface Electromyography (sEMG) [12], inertial measurement unit (IMU) [13], and Photoplethysmography (PPG) [14] sensors). However, these methods are either costly, preventing widespread deployment, or coarse-grained and have poor robustness, making it difficult to achieve highly accurate estimations. Furthermore, there is a notable lack of solutions providing workload adjustment recommendations. Overall, more research is needed to advance the level of workload estimation and adjustment guidance.

Recently, several studies have demonstrated the remarkable sensitivity of PPG signals to muscle movements, enabling applications such as chewing detection [15], gesture recognition [16], [17], and EMG estimation [18]. Inspired by them, we take one step forward by conducting on the relationship between PPG signals and workload and revealing that different workloads induce varying degrees of muscle deformations, which can be captured by a PPG sensor. Based on this, we propose a convenient, low-cost, and fine-grained FWT

monitoring system named *PPGSpotter*. It leverages infrared and green light on a PPG sensor to illuminate wrist skin and collect optical density changes containing information regarding muscle movement. By analyzing these changes, besides exercise type and repetitions, *PPGSpotter* can estimate the current workload and further predict the required workload for the next session based on the most appropriate adjustment model and training goal. Fig. 1 depicts the application scenario of the proposed system. Users only need to wear a wrist-worn device during the training process, and *PPGSpotter* can act as a private fitness spotter, monitoring the training process anytime and anywhere, further avoiding poor training or injury.

Realizing *PPGSpotter*'s idea is difficult due to three-pronged challenges. Firstly, the arterial interference induced by the highly dynamic periodic pulse signal, together with the target motion-derived signal (MDS), dominates as alternating current components in collected PPG signals. However, the two signals are heavily coupled in both time and frequency domains, making it challenging to separate them directly. Secondly, the PPG signal is sensitive to sensor position; correcting data collected at different positions and extracting effective muscle movement characterization information is challenging. Last but not least, how to simultaneously achieve multi-task inference (i.e., regressing exercise workload and classifying exercise type) from intricate muscle dynamics characterization information while accounting for each individual's personalized physiology can be highly non-trivial in practice.

To address the above challenges, we first develop an arterial interference elimination method utilizing the variable step-size normalized least mean square (VS-NLMS) to separate the MDS from arterial interference. Then, for each action segment, we generate a recurrence plot-based representation image to capture spatiotemporal information. Moreover, sensor position shift correction is designed to correct PPG signals collected at different positions. Next, we propose a multi-task CNN-based network for workload regression and exercise type classification, which can explicitly embed personal information into the learning model. Meanwhile, a decision tree is used to choose the most appropriate workload adjustment model and provide workload adjustment suggestions.

Our main contributions are listed as follows:

- We propose *PPGSpotter*, the first wearable-based FWT monitoring system that leverages a low-cost optical PPG sensor. Through the PPG sensor, *PPGSpotter* captures the subtle yet distinctive optical density fluctuations engendered by geometrical alterations of the arterial, which are elicited by deformations of specific muscle groups under varying workloads and exercise types.
- We develop a novel arterial interference elimination method that effectively reduces the impact of pulse noise.
- We design a novel spatiotemporal feature extraction method based on a recurrence plot that can resist sensor positional shifts.
- We propose a novel multi-task CNN-based learning scheme that simultaneously realizes the monitoring of workload and exercise type.

- We conduct extensive experiments with 15 participants and six types of FWT under various usage scenarios. Results show that *PPGSpotter* achieves a promising performance with an average of $0.59\,\mathrm{kg}$ RMSE for workload estimation, 0.96 reps RMSE for repetitions estimation, and 91.57% F1-score for recognizing exercise type.

II. RELATED WORK

Pioneer studies have shown that motion tracking and fitness monitoring can be achieved through various devices, including cameras [6], wearables (e.g., smart glove [19], smartwatch [5], [20], insole [21]), and wireless devices (e.g., RFID [22], Wi-Fi [23], mmWave radar [24], acoustic sensor [25], [26]). These methods, however, are merely capable of perceiving and tracking exercise types and repetitions, unable to fill the void in automatic workload sensing in the FWT process.

Recently, there have been active solutions attempting to assist in automatic recording and estimating workload, which can be broadly categorized as:

Dedicated-equipment-based solutions. The iSelect [9] is a smart dumbbell that can perform voice-controlled weight adjustments from 5 to 50 pounds. FEMO [10] utilizes RFID tags to identify the weight of each dumbbell used. However, these methods necessitate dedicated equipment such as smart dumbbells and RFID readers, incurring prohibitive costs and limiting practical adoption. W8-Scope [11] employs a simple magnetic-cum-accelerometer sensor mounted on the weight stack of exercise machines to infer various attributes of exercise behavior. However, it identifies common errors offline and without real-time feedback. Moreover, these solutions still require a high degree of cooperation from users (e.g., manually modifying the equipment or maintaining a specific range of actions), which may easily lead to poor user experience.

Wearable-device-based solutions. Compared to the aforementioned, these solutions engender more versatility by sensing users rather than equipment. For example, Muscle-Sense [12] estimates exercise workload using wearable sEMG sensors and regression analysis. Oboe et al. [27] develop a custom device with eight sEMG sensors and a 9-DoF inertial sensor to estimate the weight lifted. However, these methods rely on the not widely prevalent wearable sEMG, limiting the wide promotion of the method. Balkhi et al. [13] use an IMU, an accelerometer, and three force sensors mounted in a glove for automatic weight detection in sports activities. PaWLA [14] is a mobile weight recognition system that can classify the user's lifted weight into its corresponding label based on PPG sensors. However, these solutions are coarse-grained and perform poorly under minor weight differences, making it difficult to achieve highly accurate workload estimations. Moreover, there has yet to be a solution that has provided recommendations for corresponding workload adjustments.

To the best of our knowledge, *PPGSpotter* is the first solution to achieve personalized and full-process FWT monitoring that only leverages a PPG sensor, offering the advantage of convenience, low cost, and fine-grained.

III. PRELIMINARIES

A. Basic of PPG

PPG is an optical technique for the non-invasive detection of blood volume changes during cardiac cycles and is further used to detect blood oxygen saturation, pulse waves, and heart rates. The core principle of PPG relies on the optical properties of blood and tissue. Specifically, a typical PPG sensor employs green, red, and infrared (IR) light sources for illuminating the skin and photodiode chips for measuring the amount of backscattered light [28], [29]. Fig. 2 shows the components of the PPG signal. When the light emitted from the light source penetrates the tissues, a portion of the light is reflected by the time-varying arterial blood, and the slight fluctuations of reflected light contribute to the alternating current (AC) component while the remaining light absorbed in the venous, capillaries, skin, bones, muscles connective tissue, etc., contributing to the stable direct current (DC) component. These two components are detected as periodic optical density changes in the backscattered light, which is detected by the photodiode, forming a resultant PPG signal.
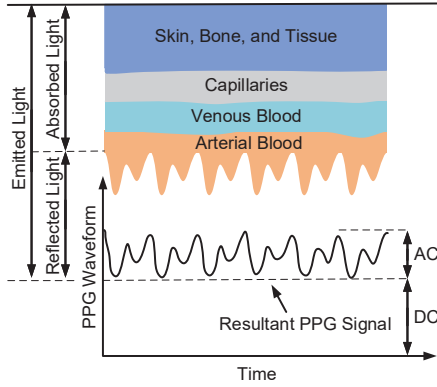
Fig. 2. The components of PPG signal.

B. Intuition of Monitoring FWT Using PPG Signals

According to exercise physiology, muscles contract (e.g., isometric, isotonic, concentric, and eccentric contraction [30]) and produce strength output to overcome a given resistance. The physiological concept of muscle contraction is based on two variables: length and tension [31], which refers to the activation of primary active muscle groups that directly participate in the movement. For example, when doing a barbell bench press and barbell biceps curl, the pectoralis major and the biceps produce a significant contraction. Muscle activation during exercise alters PPG waveforms in an exercise type- and workload-dependent manner by:

- Muscle activation increases with workloads, but this relationship is not linear [32]. Further, highly isolated forces generated in the activated musculature increase the peripheral vascular resistance and compress the arterial geometry to different degrees [33]. These can be collectively referred to as muscle tissue effects.
- PPG detects variations in blood volume pulsatile with each heartbeat; thus, changes in arterial blood flow from muscle contraction and vascular resistance alter the PPG
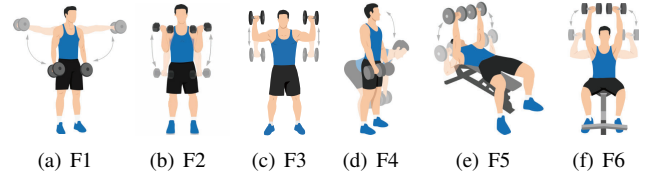
Fig. 3. An illustration of six types of free weight training: (a) F1: lateral raise; (b) F2: dumbbell curl; (c) F3: dumbbell external rotation; (d) F4: dumbbell deadlift; (e) F5: dumbbell bench press; (f) F6: seated dumbbell press.
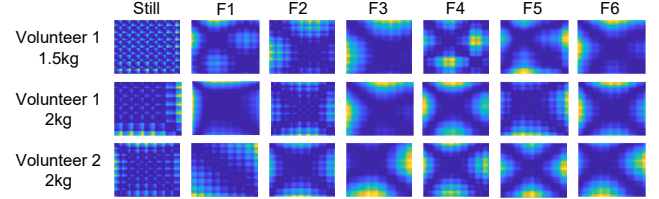
Fig. 4. The recurrence plots of PPG samples collected from different volunteers, exercise types, and workloads.

waveform. In other words, the PPG sensor can capture muscle tissue effects.

In short, the PPG signal develops a unique trend as vascular compression changes with workloads, and distinct muscle groups exhibit unique PPG signatures when activated during specific exercises. Therefore, PPG is expected to provide an inexpensive and unobtrusive modality to monitor FWT.

C. Feasibility Studies

Given the aforementioned background, we hereby conduct an experiment with two volunteers to validate the basic idea of leveraging the PPG sensor on wrist-worn devices for capturing exercise type and workload information. During the experiments, users wear an off-the-shelf PPG sensor on the radial artery placement of the right wrist and perform six types of typical dumbbell exercises (as shown in Fig. 3) with two loads (i.e., 1.5 kg and 2 kg). Note that the six free weight training are deliberately chosen to encompass a diverse range of upper-body muscle groups and movement patterns.

We extract IR PPG signals within the time window between the start and end points of each action and generate the corresponding recurrence plots, introduced in Section IV-C, as shown in Fig. 4. We can easily observe that: i) when comparing recurrence plots of PPG signals generated by different exercises, significant differences can be observed. This is because each exercise elicits specific muscle contractions and movement patterns, which influence the blood flow and subsequent PPG signal characteristics. ii) various loads applied can result in subtle differences in the PPG signals, even when considering the same user and exercise type. These differences arise due to the distinct muscle contractions associated with different loads, which exert varying effects on the compression program of blood vessels. iii) moreover, recurrence plots of PPG signals can also exhibit variations among different users due to the inherent individual differences in human physiology and vascular response, such as variations in blood vessel elasticity, tissue composition, and vascular anatomy.

Remarks: Therefore, we can conclude that the different workloads and exercise types should affect the PPG signal patterns captured in wrist-worn devices. Meanwhile, cross-user distinctions highlight the importance of personalization in FWT monitoring systems, as individual physiological characteristics should be considered to ensure accurate and reliable monitoring results.

IV. SYSTEM DESIGN

A. Overview

The basic idea of *PPGSpotter* is to utilize the optical PPG signal collected by wrist-worn devices for FWT monitoring. Fig. 5 shows the overall design of *PPGSpotter* in which the two-wavelength (infrared and green light) PPG signals are taken as the system input.

Arterial Interference Elimination is conducted to disentangle the MDS in noisy PPG signals. Specifically, we first utilize the Butterworth lowpass filter to remove high-frequency interference. Then, we calculate an arterial interference reference signal by subtracting the two-wavelength signals and conduct VS-NLMS to remove the arterial interference while extracting the pure MDS.

During *Spatiotemporal Feature Extraction*, we use the moving window to detect starting and ending points on MDS to achieve action segmentation and repetitions estimation. For each action segment, as a novel spatiotemporal feature, a recurrence plot is generated. Finally, we correct signals collected at different positions based on principal component analysis (PCA) to avoid the loss of accuracy caused by the movement of the sensor position.

In *Personalized Free Weight Training Monitoring*, we adopt a multi-task CNN-based deep learning model to simultaneously realize the monitoring of workload and exercise type. Then, the workload adjustment guidance selects the most suitable workload adjustment model according to the user's status and goals, and gives workload adjustment suggestions.

Finally, *PPGSpotter* can act as a personalized fitness spotter, achieving a convenient, low-cost, and fine-grained FWT monitoring with four results (i.e., current workload, next workload, repetitions, and exercise type).

B. Arterial Interference Elimination

To extract MDS in PPG signals, we need to remove the high-frequency and arterial interference in the collected IR PPG and Green PPG signals.

1) Signal Preprocessing: Since the PPG signal is mainly concentrated below $5\,\mathrm{Hz}$, we use a fourth-order Butterworth lowpass filter with a cutoff frequency of $5\,\mathrm{Hz}$ to remove high-frequency interference. Subsequently, the signal range is scaled to the bound $[-1, 1]$. However, there is still significant interference from the artery, which mainly refers to the highly dynamic periodic pulse signal.

2) Arterial Interference Reference Generation: The source of the PPG signal is the optical density transmitted or reflected. According to Schuster's theory [34], which is one of the basic theories of optical scattering, the relationship between
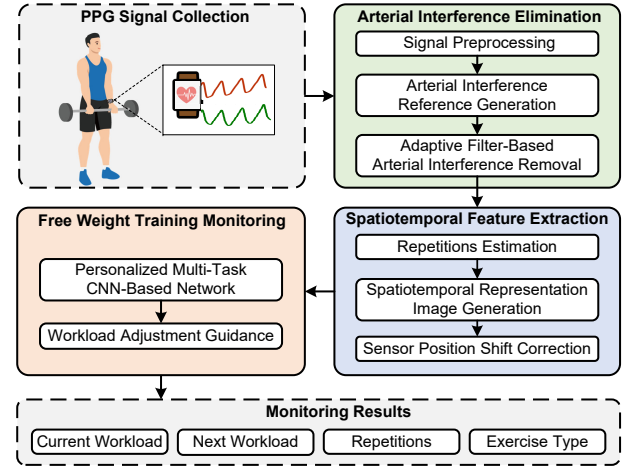

Fig. 5. System architecture of *PPGSpotter*.

the optical density changes ΔA, and blood vessel thickness changes ΔD_b for a given blood vessel can be expressed as:

$$\Delta A = [\sqrt{E_h(E_h + F)}H_b + Z_b]\Delta D_b, \tag{1}$$

where $E_h = sE_o + (1 - s)E_r$ in which E_o and E_r represent the extinction coefficients of oxyhemoglobin and deoxyhemoglobin; s represents the blood oxygen saturation. F represents the scattering coefficient. H_b is the concentration of hemoglobin in the blood. Z_b is a constant independent of the wavelength of the projected light source and approaches zero when the optical receiver is sufficiently wide.

Considering the effect of muscle tissue, one of the main sources of optical density fluctuation, Eqn. (1) is modified as [35]:

$$\Delta A = \sqrt{E_h(E_h + F)}H_b\Delta D_b + Z_b\Delta D_b + Z_t\Delta D_t, \tag{2}$$

where Z_t is a constant independent of the wavelength, and ΔD_t is the thickness change of the muscle tissue.

As shown in Fig. 2 and Eqn. (2), when the human body remains stationary, the tissue thickness change ΔD_t approaches zero. Then, the effect of tissue on the collected PPG signal is manifested as the DC component. However, the situation studied in this paper is various motions exist, and the effect of tissue is no longer constant and becomes AC component. For example, in Fig. 6(a) and Fig. 6(b), the IR and Green PPG signals have fluctuations caused by the first type of FWT (i.e., F1). Note that the two signals take on different morphologies since infrared light can penetrate the skin and reach arteries in the subcutaneous tissue, while green light can only reach superficial capillaries [28]. We face the challenge of combined AC effects of the pulse signal and MDS. Therefore, we need to treat the pulse signal as interference and separate it from the original signal to obtain a clean MDS for subsequent FWT monitoring.

Since the frequency of the MDS in motion is similar to the frequency of pulse interference, traditional methods like high-pass filtering and down-sampling will cause distortion of time domain information. Blind source separation techniques like independent component analysis (ICA) and

(a) IR PPG signal.

(b) Green PPG signal.

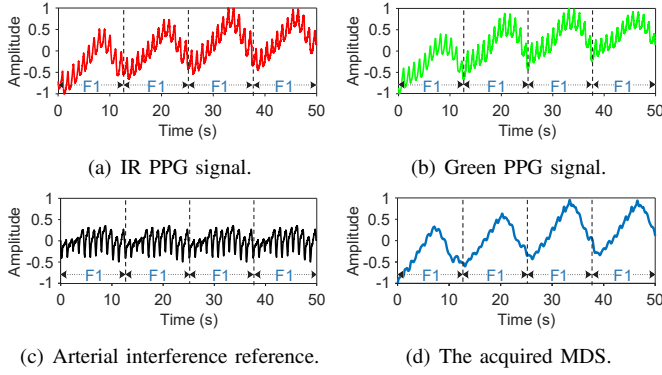(c) Arterial interference reference.

(d) The acquired MDS.

Fig. 6. An example of arterial interference elimination method.

principal component analysis (PCA) also have limitations: they struggle to accurately isolate the two mixed sources with very similar spectral content. Alternatively, adaptive filtering has the advantage of being able to adjust filter coefficients according to the characteristics of the input signal, making it suitable for handling sources with overlapping frequency content. Motivated by this, we propose an adaptive filtering method to analyze PPG patterns caused by muscle tissue effects and obtain fine-grained motion features.

Specifically, we employ two wavelengths to first cancel out the effects of Z_t and Z_b that are independent of the wavelength [35], and then obtain an arterial interference reference signal from the artery that is linearly correlated with the pulse signal. Specifically, we subtract optical densities corresponding to the two-wavelength PPG sensor:

$$\Delta A_r = \sqrt{E_h^i(E_h^i + F)}(H_b^i \Delta D_b^i) \\ - \sqrt{E_h^g(E_h^g + F)}(H_b^g \Delta D_b^g), \tag{3}$$

where i and g represent infrared and green wavelengths. This noise reference signal ΔA_r is related to the arterial vascular component and unrelated to the muscle tissue effect, as shown in Fig. 6(c). Therefore, the adaptive filter can use this interference reference signal to remove the pulse signal and obtain the desired MDS.

3) Adaptive Filter-Based Arterial Interference Removal: The LMS algorithm is widely used in signal denoising with simple principles and stable performance. However, there is a contradiction between the steady-state error and convergence rate after convergence [36]. Although the normalized LMS algorithm resolves the above contradiction by normalizing the convergence step size factor to the signal power, the fixed normalized step size factor is not conducive to better accelerated convergence. To this end, we propose VS-NLMS algorithm, which introduces an attenuation factor to make the step size factor change with the number of iterations, with both a faster convergence rate and a more effective balance of convergence rate and steady-state error.

Specifically, the expression of the step size factor is as follows:

$$\mu(n) = \frac{\beta\left(1 - exp\left(\frac{-\alpha}{n}\right)\right)}{\gamma + X^\top(k)X(k)}, \tag{4}$$

where n is the number of iterations; β is a constant that controls the convergence speed and satisfies $0 < \beta < \lambda_{max}$ (λ_{max} is the maximum eigenvalue of the auto-correlation matrix of the input signal); α is also a constant that affects the steady-state error of the algorithm; γ is a small amount between 0 and 1 to prevent the step value being too large; $X(k)$ is the input signal. The weight coefficient iteration process is as follows:

$$W(k + 1) = W(k) + 2\mu(n)e(k)X(k), \tag{5}$$

where e represents the error. Specifically, we focus on noise removal analysis in IR PPG signals since it can better capture muscle tissue movement information during motions. As a result, the acquired MDS is solely represented by one channel, as illustrated in Fig. 6(d).

C. Spatiotemporal Feature Extraction

The shift in sensor position can significantly distort the acquired PPG waveforms [37] and completely overwhelm the exercise- and workload-specific PPG patterns, making FWT monitoring task highly susceptible to positional noise. We focus on extracting nuanced spatial dynamics by generating a recurrence plot to map each PPG segment into a two-dimensional phase space. Rotational alignment of the recurrence plot axes then allows us to disentangle the positional and exercise factors projecting out the spatial artifacts while retaining the core exercise dynamics along the aligned axes. The recurrence plot provides an information-rich representation, while the alignment imposes spatial invariance critical for generalization.

1) Repetitions Estimation: We design an improved moving window method to detect valley values of MDS, segment the signal based on the signal period, and obtain repetitions. Specifically, we locate the first valley v_1 according to *findpeaks* algorithm [38], use auto-correlation algorithm [39] to calculate the period p_1 of the signal in the first 15 seconds, and set initial value of jump step t as p_1. Then, the position of the second valley v_2 is detected by finding the minimum among data points of which abscissa is within the scope of $t/3$ from $v_1 + t$, and then updating the jump step $t = v_2 - v_1$, and so on. The improved moving window method uses skip-detection, thus reducing computational complexity. Meanwhile, updating the detection window's jump step and length in real-time based on the current period makes the improved algorithm more stable and accurate.

2) Spatiotemporal Representation Image Generation: Recurrence plot is an innovative visualization technique that unravels the hidden recurrent patterns and complex dynamics in time series data. In this work, we construct a recurrence plot for each PPG segment, which provides two major advantages tailored for exercise analysis: First, the recurrence plot encodes the temporal dependencies and spatial fluctuations of the PPG waveform, thus preserving critical spatiotemporal information for estimating workload and recognizing exercise types. Second, the 2D image representation enables the extraction of
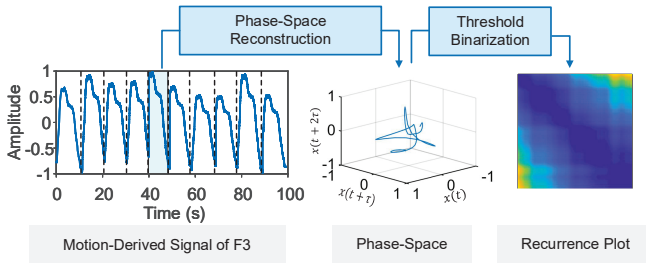
Fig. 7. The process of recurrence plot generation.

spatiotemporal features using CNN, allowing robust feature learning without cumbersome feature engineering.

Fig. 7 shows the process of recurrence plot generation. Firstly, we transform each point p_m in the time series into the corresponding state $\vec{s_m}$ in the phase space. Then, the distance (vector norm) between every two states is calculated. Next, threshold binarization is performed to obtain the characteristics between two corresponding states in the recurrence plot. In short, the primary idea of recurrence plot is to disclose the trajectory movements from the current state to the previous state, and it can be formulated as:

$$R_{m,n} = \theta(\epsilon - \|\vec{s_m} - \vec{s_n}\|), m, n = 1, \ldots, Q, \quad (6)$$

where Q is the number of states $\vec{s}$; $R_{m,n}$ is a $Q \times Q$ square matrix; ϵ is a threshold value for determining the neighborhood of states; θ is the Heaviside (step) function. The recurrence matrix R contains two sets of values called textures and typologies. The texture information belongs to single dots, diagonals, vertical lines, and horizontal lines. The typology information is classified into homogeneous, regular, drifting, and disrupted types.

3) Sensor Position Shift Correction: Through repeated experiments, we can find that under the premise of the same user, workload, and action, there are differences in curve shape and signal amplitude of PPG signals collected from different positions of the wrist. Generated recurrence plots also exhibit obvious and complex rotation phenomena. Therefore, we propose to calibrate signals collected at different positions to have similar recurrence plot representations based on PCA. This approach can align each recurrence plot's axes to its principle directions and ensure that the variance is maximal in the direction of rows or columns, thus resisting sensor positional shifts.

Specifically, we first record the recurrence plots from multiple sensor positions and find the center of gravity (x_c, y_c) for each recurrence plot, which can be expressed as:

$$x_c = \frac{\sum_I \sum_J j \cdot p(i,j)}{\sum_I \sum_J p(i,j)}, y_c = \frac{\sum_I \sum_J i \cdot p(i,j)}{\sum_I \sum_J p(i,j)}, \quad (7)$$

where I and J represent the number of columns and rows; $p(i,j)$ is the pixel value. Then, we establish two-dimension coordinate system on the center of gravity as the origin and record all the coordinates (x_i, y_i) (where x_i and y_i are the number of columns and rows) in which the gray value of the recurrence plot image is not 0. Next, for each image, all

the coordinates in rows are arranged and formed an $N \times 2$ matrix L. To perform feature centering on L, the mean of each column is calculated and then subtracted from each element in the dataset, respectively, resulting in a new dataset $L1$. Then, we calculate a relevant covariance matrix S_{L1} and two orthonormal eigenvectors with two eigenvalues that are associated with each other:

$$S_{L1} = \frac{1}{N-1} L1^\top L1. \quad (8)$$

In the 2D coordinate space, each feature vector calculated by Eqn. (8) is 2D, reflecting a straight line in the space. These two feature vectors are orthogonal, thus forming a new coordinate system where points along one direction have max feature variance and along the other direction have min feature variance. For consistency, the original coordinate system is rotated by the smallest angle to align with the new coordinate system and make the vertical direction have the maximum feature variance. Then the directions of feature vectors are adjusted according to the current coordinate system directions, yielding a new feature vector matrix V. Nest, for each pixel of rotated image, use inverse transformation $[x_i'', y_i''] = [x_i', y_i'] \cdot V^{-1}$, where $[x_i', y_i']$ represents a pixel in the rotated image, and $[x_i'', y_i'']$ represents a pixel in the original image, to find the corresponding pixel of the original image. Finally, we employ bilinear interpolation to fill in the missing pixel points and resize each image to 128×128 resolution. This process ensures consistency and uniformity across all images. Finally, we can get a corrected image for each original recurrence plot image.

D. Personalized Free Weight Training Monitoring

We design a novel multi-task CNN framework for workload regression and exercise type classification. This approach automatically extracts robust feature representations from input recurrence plots without relying on predefined manual features or expert knowledge. A key innovation is the explicit incorporation of personal information (age, gender, height, and weight) into the learning model, enabling consideration of individual physiological characteristics for accurate and reliable results. Additionally, we construct a decision tree to select the optimal workload adjustment model based on exercise type and current workload level, further enhancing the system's performance.

1) Multi-Task CNN-Based Network: Fig. 8 shows the proposed multi-task CNN-based network. The recurrence plot for each action segment of MDS is the input of the CNN-based network. In addition, we incorporate the user's personal information (i.e. age, gender, height, and weight) into the learning model to achieve a personalized FWT monitoring framework. Besides the six exercise types, we also define a *NULL* class to represent unknown exercise types outside the defined classes, such as the extra actions caused by switching between actions. The output contains class labels and the estimated workload (estimation results for *NULL* classes will be discarded).

Given that the appearance of recurrence plots is usually globally similar and locally different, both global and local
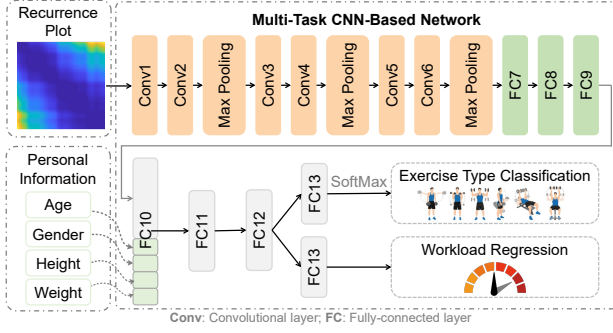
Fig. 8. The multi-task CNN-based deep learning framework.

structural information are important for classification and regression tasks. To capture the local structural information of recurrence plots, six convolution blocks are used; each block involves a 2D-convolution layer using a rectified linear unit (ReLU) activation function. The six convolution layers use 32, 32, 64, 64, 128, and 128 kernels, respectively, and the kernel sizes are 3×3. Specifically, Conv2, Conv4, and Conv6 are followed by $2 \times 2 \times 2$ max pooling layers for down-sampling to learn the locally salient information. Two fully-connected (FC) layers (i.e., FC7 and FC8) are with 128 and 64 units.

We then add two additional FC layers (i.e., FC9 and FC10) with 64 and 68 units to model the global structural information of recurrence plots. In addition, the cascaded representation of the output of FC10 and the personal information (i.e., age, gender, height, and weight) are fed into two FC layers (i.e., FC11 and FC12 with 64 units). Finally, two FC13 layers with 32 units are used to predict the class probability through *Softmax* and estimating the workload, respectively.

The objective function of the proposed CNN-based network is as follows:

$$argmin - \frac{1}{C} \sum_{c=1}^{C} \frac{1}{N} \sum_{X_n \in \mathcal{X}} 1\left\{y_n^c = c\right\} log\left(P(y_n^c = c|X_n)\right)$$
$$+ \frac{1}{N} \sum_{X_n \in \mathcal{X}} (z_n^s - \widetilde{z}_n^s)^2, \tag{9}$$

where $\mathcal{X} = \{X_n\}_{n-1}^{N}$ denotes the training set including N

TABLE I
FOUR FREQUENTLY-USED WORKLOAD ADJUSTMENT MODELS.

| Model Name	Basic Description
Linear loading [40]	(i) Increase load by fixed value each session (ii) Inputs: current load, increment
Two-for-two rule [41]	(i) Increase load if two more reps are completed over the recommended goal during two consecutive training sessions (ii) Inputs: current load, rep range, increment
Pyramid rule [42]	(i) Begin with lighter loads and higher reps, then gradually decreases reps and increase workload (ii) Inputs: current load, 1RM, rep ranges, increment or decrement
RM zones [43]	(i) Select the heaviest load that can be lifted for a given repetition range with the goal of reaching muscular failure on the final set of the exercise (ii) Inputs: current load, RM Range, 1RM, load-rep relationship charts
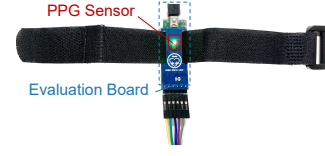
Fig. 9. *PPGSpotter* prototype.

recurrence plots. $C = 6$ represents six different exercise types. $1\{\cdot\}$ is an indicator function, with a value of 1, if $\{\cdot\}$ is true; and 0, otherwise. $P(y_n^c = c|X_n)$ indicates the probability of X_n being correctly classified as the category y_n^c. z_n^s and $\widetilde{z}_n^s$ are estimated workload and the ground truth, respectively. In short, the first term is the cross-entropy loss for multi-class exercise type classification, and the second one is the mean squared loss for regression to evaluate the difference between the estimated workload and the ground truth.

2) Workload Adjustment Guidance: Optimizing workload management is imperative to continually induce physiological adaptation, thus avoiding poor training or injury. However, finding the ideal workload adjustment model remains challenging due to individual differences. To address this, we propose a decision tree scheme to automatically choose one of four frequently-used workload adjustment models, which consist of linear loading, the two-for-two rule, pyramid rule, and repetition maximum (RM) zones based on the user's status.

Specifically, the decision nodes include the user's experience level (beginner or advanced), recent training effectiveness (progress or plateau), and targeted training goal (hypertrophy or strength). Each node contains binary categories. The decision tree is built via a recursive partitioning process based on these nodes and values. For beginner trainees (i.e., defined as individuals with less than three months of training age), linear loading with fixed inter-session increments is recommended. The two-for-two rule is appropriate if the advanced user continues making gains. When plateaued, pyramid rule is suggested for hypertrophy goals, while RM zones are optimal for further strength gains. We compare the key features of each model in Table I.

While simplistic models like linear loading can suffice for novices, complex models may obviously enhance efficiency and continued progress for advanced users. *PPGSpotter* allows for hierarchical decision-making as the user becomes more proficient with an individual's changing status and goals.

V. EVALUATION

A. Experimental Methodology

1) Implementation: In our proof-of-concept implementation, we build a prototype consisting of an off-the-shelf PPG sensor (with green and infrared light) and an embedded evaluation board as a smartwatch alternative, as shown in Fig. 9. During the FWT process, the PPG sensor readings are recorded with a sampling rate of $200\,\mathrm{Hz}$, and an experienced fitness coach is arranged in front of the participants to record the ground truth.
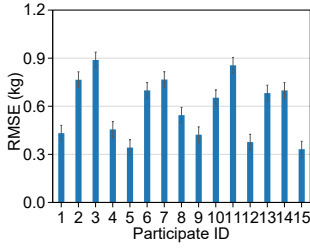
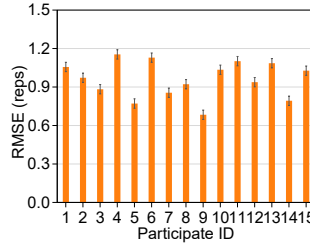Fig. 10. Overall performance of workload estimation.

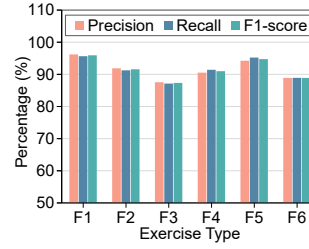Fig. 11. Overall performance of repetitions estimation.

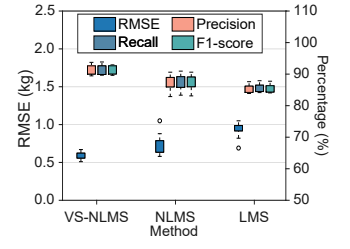Fig. 12. Overall performance of exercise type classification.

Fig. 13. Impact of adaptive filtering method.

2) Data Collection: We recruit 15 participants, including 8 males and 7 females (aged between 19 and 42), to conduct six types of FWT for evaluation. Their training ages range from 0 to 6 years. In particular, we include 5 participants with no fitness experience to verify that our approach is appropriate for not only gym enthusiasts but also regular users. This study is conducted with the approval of our institute's IRB. After a brief training session on standard action, we ask participants to wear the prototype closely on the radial, center, and ulnar zone placement of their right wrist, respectively. For each participant, we first determine their 1RM for each exercise type through standardized strength testing protocols. Based on these results, we define a personalized 60%-80% 1RM range (incremented in 0.5 kg) as the workload collection interval for that individual. The entire data collection process takes one month, and we finally collect over $5,000$ repetitions of each participant for training and evaluation.

3) Evaluation Metrics: We utilize the following metrics to evaluate the performance of *PPGSpotter*:

Root Mean Squared Error (RMSE). The standard deviation of the workload or repetitions prediction errors, which is defined as $\sqrt{\frac{1}{n}\sum_{i=1}^{n}(\hat{y}_i - y_i)^2}$, where n is the number of samples, y_i is the ground truth value, and $\hat{y}_i$ is the predicted value of workload or repetitions. Lower values of RMSE indicate better estimation accuracy.

Precision. The percentage of the action segments correctly recognized as type A among all the number of segments predicted as the action type A.

Recall. The percentage of the segments that are correctly recognized as the action type A among all segments of the action type A.

F1-score. The harmonic mean of precision and recall, which is defined as $F_1 = 2 \cdot \frac{recall \cdot precision}{recall + precesion}$, where an F1-score reaches its best value at 1 and worst at 0.

B. Overall Performance

To evaluate the overall performance of *PPGSpotter*, we conduct experiments with all participants performing six types of exercises (as shown in Fig. 3). Specifically, personalized models are built for each participant. Moreover, we use 80% of the data for training, the rest 20% for testing, and conduct five-fold cross-validation.

1) Workload Estimation Performance: Fig. 10 presents the RMSE for workload estimation across all 15 participants. We can find that the RMSE results range from 0.32 kg to 0.89 kg

across participants, indicating accurate workload prediction with an average error of 0.59 kg. In particular, participants #5 and #15 have the lowest estimation errors. This could be because they likely have relatively rich fitness experience and standard exercise forms, which allow the sensor to capture more stable and reliable information during the FWT process.

2) Repetitions Estimation Performance: Fig. 11 presents the RMSE for repetitions estimation across all 15 participants. We can find that the RMSE results vary between 0.68 reps and 1.15 reps, with an average error of 0.96 reps. This indicates *PPGSpotter* can reliably track repetitions during FWT process, with most participants obtaining errors below 1 rep per set on average. Overall, the low average RMSE demonstrates the robust performance of *PPGSpotter* in counting exercise repetitions in varied realistic scenarios.

3) Exercise Type Classification Performance: We report the average precision, recall, and F1-score for recognizing the six types of FWT in Fig. 12. For each type, we calculate the average value among different participants. Overall, *PPGSpotter* achieves mean precision of 91.55%, recall of 91.59%, and F1-score of 91.57%, indicating accurate recognition of exercise types. All exercise types receive F1-scores above 85%, demonstrating reliable recognition. In addition, F3 (dumbbell external rotation) and F6 (seated dumbbell press) have more similar motion patterns, resulting in F1-score lower than 90%.

C. Key Algorithms Study

1) Impact of Adaptive Filter Methods for Arterial Interference Elimination: We compare our proposed variable step-size normalized LMS (VS-NLMS) against standard LMS and NLMS filters for adaptive filter-based arterial interference elimination tasks. Fig 13 shows the box plot of workload estimation and exercise type classification results for each method. Specifically, VS-NLMS achieves an average RMSE of 0.59 kg for workload estimation, significantly lower than NLMS (0.72 kg) and LMS (0.93 kg). Additionally, for exercise type classification, VS-NLMS attains the highest average F1-score of 91.57%, compared to 87.20% for NLMS and 85.05% for LMS. This demonstrates that VS-NLMS successfully suppresses erratic arterial noise for accurate workload estimation and exercise type classification, validating the effectiveness of our proposed interference elimination technique.

2) Effectiveness of Sensor Position Shift Correction: To evaluate the effectiveness of our proposed algorithm in correcting sensor shifts, we compare workload estimation and
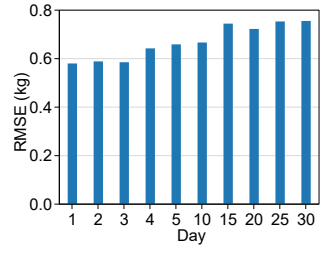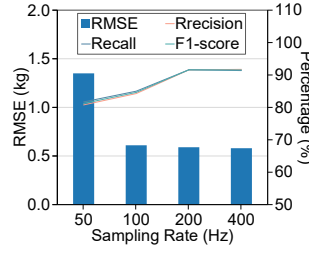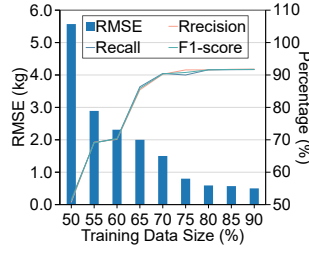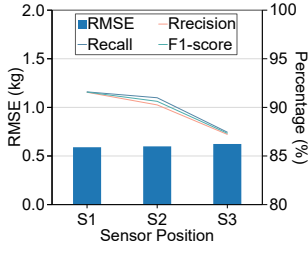
Fig. 14. Impact of sensor position. Fig. 15. Impact of training data size. Fig. 16. Impact of sampling rate. Fig. 17. Long-term performance

exercise type classification performance across three sensor positions of the right volar wrist (S1: radial zone, S2: center zone, S3: ulnar zone). As shown in Fig 14, our proposed image calibration algorithm demonstrates consistent performance across different sensor positions on the wrist. Specifically, the workload estimation REMS remains lower than $0.65\,$kg regardless of the sensor shifts from the radial zone to the ulnar zone of the volar wrist. Furthermore, the exercise type classification accuracy shows a minimal variation ($<3\%$) between the three sensor positions tested. These indicate that image calibration generalizes well and retains robustness power for workload estimation and exercise type classification.

3) Performance of Multi-Task CNN-Based Network: We compare the impact of training data size on system performance by varying the training data size from 50% to 90%. Specifically, we incrementally increase the training data in 5% increments, training the model each time for each participant. We then test on the remaining data sets and record the results. The results are shown in Fig. 15, which demonstrate that as training data increases, RMSE of workload estimation steadily decreases from around $5.57\,$kg to $0.50\,$kg; F1-score of exercise type classification increases from around 51.21% to 91.66%. After 80% of the training data size, the CNN-based network achieves lower than $0.60\,$kg RMSE and higher than 91% F1-score, which supports our choice of 80% training data for CNN in the experiments for making an optimal trade-off between data training time and accuracy.

D. Impact of Sampling Rate

The sampling rate is closely linked with the system performance, for low sampling rates probably reduce the recognition performance, while high sampling rates bring greater time costs. We evaluate *PPGSpotter* specifically under several different sampling rates including $50\,$Hz, $100\,$Hz, $200\,$Hz, and $400\,$Hz. Fig. 16 shows the RMSE of workload estimation and precision, recall, and F1-score of exercise type classification at the above sampling rates. We can observe that the system performance improves continuously when the sampling rate increases from $50\,$Hz to $200\,$Hz. However, the improvement is no longer significant when the sampling rate reaches around 200 Hz. The results indicate that the workload estimation and exercise type classification achieve pretty exceptional performance with the RMSE of $0.59\,$kg and precision, recall, F1-score of 91.55%, 91.59%, and 91.57% when *PPGSpotter* uses a sampling rate of $200\,$Hz. Thus, $200\,$Hz is adopted in this work.

E. Long-Term Performance

Long-term studies can provide insights into potential challenges, such as muscle growth and body dimension changes, allowing us to refine the system accordingly. Over a one-month period, we periodically evaluate *PPGSpotter*'s performance by testing it on new data from each participant collected at 1, 2, 3, 4, 5, 10, 15, 20, 25, and 30 days, and the results are shown in Fig. 17. Particularly, we update the training data and personal information by collecting new examples every week. With this updated training data, *PPGSpotter* maintains a workload estimation RMSE under $0.8\,$kg across the evaluation period. The results highlight the importance of updating training data periodically to account for long-term changes in input data distribution. Overall, *PPGSpotter* demonstrates satisfactory robustness and stability on long-term testing.

VI. CONCLUSION AND FUTURE WORK

This paper proposes *PPGSpotter*, the first FWT monitoring system that relies on PPG sensors available in ubiquitous wrist-worn devices. It tracks optical density change caused by the muscle tissue deformation during exercise execution and achieves fine-grained monitoring of current workload, repetitions, and exercise type. More importantly, *PPGSpotter* provides users with personalized recommendations for workload adjustment, enhancing training efficacy and reducing the risk of injury. To extract the MDS from the PPG signal, we propose an arterial interference elimination method to eliminate the highly dynamic periodic pulse signal interference. Then, we introduce a recurrence plot-based representation extraction method that captures spatiotemporal information and resists shift of the sensor position. To enable personalized monitoring, we design a multi-task CNN-based learning scheme that incorporates users' basic information and simultaneously performs workload regression and exercise type classification. Additionally, the workload adjustment guidance model is designed to select the most suitable workload adjustment model, further providing next workload suggestions. Through extensive experiments involving 15 participants and six types of FWT, we demonstrate the practical usability of *PPGSpotter*.

Future plans for *PPGSpotter* involve exploring the influence of other gravity-resistant devices, such as barbells and kettlebells. Investigating the effect of such device-related exercises on *PPGSpotter* can provide valuable insights into its applicability and limitations in different exercise modalities.

REFERENCES

[1] C. G. Abildso, S. M. Daily, M. R. U. Meyer, C. K. Perry, and A. Eyler, "Prevalence of Meeting Aerobic, Muscle-Strengthening, and Combined Physical Activity Guidelines During Leisure Time Among Adults, by Rural-Urban Classification and Region—United States, 2020," *American Journal of Transplantation*, vol. 23, no. 3, pp. 443–446, 2023.

[2] S. E. Gray and C. F. Finch, "The Causes of Injuries Sustained at Fitness Facilities Presenting to Victorian Emergency Departments-Identifying The Main Culprits," *Injury Epidemiology*, vol. 2, no. 1, pp. 1–8, 2015.

[3] S. C. Glass and D. R. Stanton, "Self-Selected Resistance Training Intensity in Novice Weightlifters," *The Journal of Strength & Conditioning Research*, vol. 18, no. 2, pp. 324–327, 2004.

[4] Y. Xie, F. Li, Y. Wu, and Y. Wang, "Hearfit: Fitness Monitoring on Smart Speakers via Active Acoustic Sensing," in *Proc. of IEEE INFOCOM*, 2021, pp. 1–10.

[5] X. Guo, J. Liu, and Y. Chen, "FitCoach: Virtual Fitness Coach Empowered by Wearable Mobile Devices," in *Proc. of IEEE INFOCOM*, 2017, pp. 1–9.

[6] R. Khurana, K. Ahuja, Z. Yu, J. Mankoff, C. Harrison, and M. Goel, "Gymcam: Detecting, Recognizing and Tracking Simultaneous Exercises in Unconstrained Scenes," *Proc. of ACM IMWUT*, vol. 2, no. 4, pp. 1–17, 2018.

[7] B. J. Mortazavi, M. Pourhomayoun, G. Alsheikh, N. Alshurafa, S. I. Lee, and M. Sarrafzadeh, "Determining The Single Best Axis for Exercise Repetition Recognition and Counting on Smartwatches," in *Proc. of IEEE BSN*, 2014, pp. 33–38.

[8] D. P. Swain, "Energy Cost Calculations for Exercise Prescription: An Update," *Sports Medicine*, vol. 30, pp. 17–22, 2000.

[9] NordicTrack, "Iselect Voice-Controlled Dumbbells," 2023. [Online]. Available: https://www.nordictrack.com/strength-training/iselect-voice-controlled-dumbbells

[10] H. Ding, L. Shangguan, Z. Yang, J. Han, Z. Zhou, P. Yang, W. Xi, and J. Zhao, "FEMO: A Platform for Free-Weight Exercise Monitoring with RFIDs," in *Proc. of ACM SenSys*, 2015, pp. 141–154.

[11] M. Radhakrishnan, A. Misra, and R. K. Balan, "W8-Scope: Fine-Grained, Practical Monitoring of Weight Stack-Based Exercises," *Pervasive and Mobile Computing*, vol. 75, p. 101418, 2021.

[12] C. G. Lim, C. Y. Tsai, and M. Y. Chen, "MuscleSense: Exploring Weight Sensing Using Wearable Surface Electromyography (sEMG)," in *Proc. of ACM TEI*, 2020, pp. 255–263.

[13] P. Balkhi and M. Moallem, "A Multipurpose Wearable Sensor-Based System for Weight Training," *Automation*, vol. 3, no. 1, pp. 132–152, 2022.

[14] A. M. Rahman, P. Wang, W. Wang, and Y. Wang, "PaWLA: PPG-Based Weight Lifting Assessment," in *Proc. of IEEE IPCCC*, 2022, pp. 130–137.

[15] V. Papapanagiotou, C. Diou, L. Zhou, J. van den Boer, M. Mars, and A. Delopoulos, "A Novel Chewing Detection System Based on PPG, Audio, and Accelerometry," *IEEE Journal of Biomedical and Health Informatics*, vol. 21, no. 3, pp. 607–618, 2016.

[16] T. Zhao, J. Liu, Y. Wang, H. Liu, and Y. Chen, "PPG-Based Finger-Level Gesture Recognition Leveraging Wearables," in *Proc. of IEEE INFOCOM*, 2018, pp. 1457–1465.

[17] Y. Zhang, T. Gu, C. Luo, V. Kostakos, and A. Seneviratne, "FinDroidHR: Smartwatch Gesture Input with Optical Heartrate Monitor," *Proc. ACM Interact. Mob. Wearable Ubiquitous Technol.*, vol. 2, no. 1, mar 2018. [Online]. Available: https://doi.org/10.1145/3191788

[18] M. Okamoto and K. Murao, "PPG2EMG: Estimating Upper-Arm Muscle Activities and EMG from Wrist PPG Values," *Sensors*, vol. 23, no. 4, p. 1782, 2023.

[19] Y. Zou, D. Wang, S. Hong, R. Ruby, D. Zhang, and K. Wu, "A Low-Cost Smart Glove System for Real-Time Fitness Coaching," *IEEE Internet of Things Journal*, vol. 7, no. 8, pp. 7377–7391, 2020.

[20] T. Zheng, C. Cai, Z. Chen, and J. Luo, "Sound of Motion: Real-time Wrist Tracking with A Smart Watch-Phone Pair," in *Proc. of IEEE INFOCOM*. IEEE, 2022, pp. 110–119.

[21] D. S. Elvitigala, D. J. Matthies, L. David, C. Weerasinghe, and S. Nanayakkara, "GymSoles: Improving Squats and Dead-Lifts by Visualizing The User's Center of Pressure," in *Proc. of ACM CHI*, 2019, pp. 1–12.

[22] R. Chaudhri, J. Lester, and G. Borriello, "An RFID Based System for Monitoring Free Weight Exercises," in *Proc. of ACM SenSys*, 2008, pp. 431–432.

[23] Y. Zhu, D. Wang, R. Zhao, Q. Zhang, and A. Huang, "FitAssist: Virtual Fitness Assistant Based on WiFi," in *Proc. of ACM MobiQuitous*, 2019, pp. 328–337.

[24] Y. Xie, R. Jiang, X. Guo, Y. Wang, J. Cheng, and Y. Chen, "MmFit: Low-Effort Personalized Fitness Monitoring Using Millimeter Wave," in *Proc. of IEEE ICCCN*, 2022, pp. 1–10.

[25] Y. Xie, F. Li, Y. Wu, and Y. Wang, "Hearfit+: Personalized Fitness Monitoring via Audio Signals on Smart Speakers," *IEEE Transactions on Mobile Computing*, 2021.

[26] C. Cai, R. Zheng, and J. Luo, "Ubiquitous Acoustic Sensing on Commodity IoT Devices: A Survey," *IEEE Communications Surveys & Tutorials*, vol. 24, no. 1, pp. 432–454, 2022.

[27] R. Oboe, A. Tonin, K. Yu, K. Ohnishi, and A. Turolla, "Weight Estimation System Using Surface EMG Armband," in *Proc. of IEEE ICIT*, 2017, pp. 688–693.

[28] Y. Cao, H. Chen, F. Li, and Y. Wang, "Crisp-BP: Continuous Wrist PPG-Based Blood Pressure Measurement," in *Proc. of ACM MobiCom*, 2021, pp. 378–391.

[29] Y. Cao, Q. Zhang, F. Li, S. Yang, and Y. Wang, "PPGpass: Nonintrusive and Secure Mobile Two-Factor Authentication via Wearables," in *Proc. of IEEE INFOCOM*, 2020, pp. 1917–1926.

[30] M. Roig, K. O'Brien, G. Kirk, R. Murray, P. McKinnon, B. Shadgan, and W. Reid, "The Effects of Eccentric versus Concentric Resistance Training on Muscle Strength and Mass in Healthy Adults: A Systematic Review with Meta-Analysis," *British Journal of Sports Medicine*, vol. 43, no. 8, pp. 556–568, 2009.

[31] C. R. Bagshaw, *Muscle Contraction*. Springer Science & Business Media, 1993.

[32] R. van den Tillaar, V. Andersen, and A. H. Saeterbakken, "Comparison of Muscle Activation and Kinematics during Free-Weight Back Squats with Different Loads," *PLoS One*, vol. 14, no. 5, p. e0217044, 2019.

[33] A. Albright, M. Franz, G. Hornsby, A. Kriska, D. Marrero, I. Ullrich, and L. S. Verity, "American College of Sports Medicine Position Stand. Exercise and Type 2 Diabetes." *Medicine and Science in Sports and Exercise*, vol. 32, no. 7, pp. 1345–1360, 2000.

[34] T. Aoyagi, M. Fuse, N. Kobayashi, K. Machida, and K. Miyasaka, "Multiwavelength Pulse Oximetry: Theory for The Future," *Anesthesia & Analgesia*, vol. 105, no. 6, pp. S53–S58, 2007.

[35] R. Yousefi, M. Nourani, S. Ostadabbas, and I. Panahi, "A Motion-Tolerant Adaptive Algorithm for Wearable Photoplethysmographic Biosensors," *IEEE Journal of Biomedical and Health Informatics*, vol. 18, no. 2, pp. 670–681, 2013.

[36] Y. Wu, Y. Xie, and H. Ge, "An Improved Adaptive Filtering Algorithm for ECG Signals," in *Proc. of the IEEE ICCCS*, 2022, pp. 354–357.

[37] Y. Maeda, M. Sekine, and T. Tamura, "Relationship Between Measurement Site and Motion Artifacts in Wearable Reflected Photoplethysmography," *Journal of medical systems*, vol. 35, pp. 969–976, 2011.

[38] PyPI, "Findpeaks," 2023. [Online]. Available: https://pypi.org/project/findpeaks/

[39] D. M. Rubin, "A Simple Autocorrelation Algorithm for Determining Grain Size from Digital Images of Sediment," *Journal of Sedimentary Research*, vol. 74, no. 1, pp. 160–165, 2004.

[40] S. Fleck, "Non-Linear Periodization for General Fitness & Athletes," *Journal of Human Kinetics*, vol. 29, no. Special-Issue, pp. 41–45, 2011.

[41] T. J. Suchomel, S. Nimphius, C. R. Bellon, W. G. Hornsby, and M. H. Stone, "Training for Muscular Strength: Methods for Monitoring and Adjusting Training Intensity," *Sports Medicine*, vol. 51, no. 10, pp. 2051–2066, 2021.

[42] D. C. Cardozo and D. de Souza Destro, "Pyramidal Resistance Training–A Brief Review of Acute Responses and Long-term Adaptations," *Journal of Bodywork and Movement Therapies*, vol. 35, pp. 21–27, 2023.

[43] G. E. Campos, T. J. Luecke, H. K. Wendeln, K. Toma, F. C. Hagerman, T. F. Murray, K. E. Ragg, N. A. Ratamess, W. J. Kraemer, and R. S. Staron, "Muscular Adaptations in Response to Three Different Resistance-Training Regimens: Specificity of Repetition Maximum Training Zones," *European Journal of Applied Physiology*, vol. 88, pp. 50–60, 2002.